Heliyon 9 (2023) e18379

Contents lists available at ScienceDirect

Heliyon

journal homepage: www.cell.com/heliyon

Dynamic analysis of thick plates reinforced with agglomerated GNPs

Ali Alnujaie [a], Mohammad Yahya Alshahrani [b], Wessim Salahaddin Ibrahim [c], Yaser Yasin [d], Zahraa Salam Obaid [e], Israa J. Alhani [f], Mohammad Hasan Khaddour [g], Salema K. Hadrawi [h], Yaassin Riyahi [i,*], M.H. Ghazwani [a]

[a] Mechanical Engineering Department, Faculty of Engineering, Jazan University, P.O.Box 45142, Jazan, Kingdom of Saudi Arabia
[b] Department of Clinical Laboratory Sciences, College of Applied Medical Sciences, King Khalid University, Abha, Saudi Arabia
[c] Department of Pharmacy, AlNoor University College, Bartella, Iraq
[d] College of Medical Technology, Al-Farahidi University, Iraq
[e] Building and Construction Engineering Technology Department, AL-Mustaqbal University College, Hillah 51001, Iraq
[f] Mazaya University College, Iraq
[g] Al-Amarah University College, Al-Amarah, Iraq
[h] Refrigeration and Air-conditioning Technical Engineering Department, College of Technical Engineering, The Islamic University, Najaf, Iraq
[i] An Independed Researcher, Iraq

A R T I C L E I N F O

Keywords:
Free vibration
Forced vibration
Rectangular plate
Graphene nanoplatelets (GNPs)
Agglomeration

A B S T R A C T

In this work, the quasi-3D hyperbolic shear deformation theory (quasi-3D HSDT) is utilized to examine the dynamics of thick rectangular plates reinforced with rectangular nanofillers known as graphene nanoplatelets (GNPs). Agglomeration of the GNPs is incorporated and the mechanical characteristics like shear, elastic, and bulk moduli, Poisson's ratio, and density are analysed according to the mixture along with the Eshelby-Mori-Tanaka approach. Hamilton's principle is hired to derive the solving equations, the Navier approach is hired to present an analytical solution in the spatial domain, and the Newmark method is hired to provide an approximate solution in the time domain. The relevance of the dynamic response and the natural frequencies of the plate on several parameters are explored such as dispersion pattern and the GNPs percentage and agglomeration parameters. It is discovered that for a specific GNPs percentage, growth in the amount of agglomerated GNPs leads to lower natural frequencies and higher dynamic deflection. Meanwhile, for a specific mass fraction of the agglomerated GNPs, growth in the volume of clusters brings about higher natural frequencies and lower dynamic deflection.

1. Introduction

Because of the unique electrical and thermo-mechanical properties, nanofillers (carbon nanotubes (CNTs) and graphene nanoplatelets (GNPs)) could be applied as reinforcement in polymer-based structures known as nanocomposites [1,2]. In comparison with a CNT, a GNP benefits from an extended surface area and more powerful bonding with the polymer, thus, in the same mass fraction, using GNPs brings about better mechanical characteristics such as higher fracture toughness, higher elastic modulus, higher tensile

* Corresponding author.
E-mail address: yaassinriyahi@gmail.com (Y. Riyahi).

https://doi.org/10.1016/j.heliyon.2023.e18379
Received 25 February 2023; Received in revised form 2 June 2023; Accepted 16 July 2023
Available online 17 July 2023

strength, and also better fatigue behavior [3]. The nanocomposites enriched with GNPs have been widely utilized in different industries [4–6]. In recent years, a considerable number of works are published to explore the impacts of GNPs on the mechanical action of nanocomposites. In two similar papers, Song et al. [7,8] explored the bending, buckling, and vibrational actionof a plate enriched with GNPs. They discussed the impacts of the dispersion pattern, dimensions, and GNPs percentage on the dynamic and static deflections, natural frequencies, and buckling loads of such a structure. Barati and Zenkour [9] explored the free vibration of a porous nanocomposite cylindrical shell enriched with GNPs. They examined the relevance of the natural frequencies on the dimensions and dispersion pattern of the GNPs. It was shown in Refs. [7–9] that when a small amount of GNPs are subjoined to the polymer, the mechanical characteristics of the structures are dramatically improved which includes reductions in the dynamic and static deflections and growth in the natural frequencies and buckling loads. The size-dependent nonlinear mechanical postbuckling analysis of a porous microplate enriched with GNPs was verified by Sahmani et al. [10]. They reported an improvement in the postbuckling characteristics of such a structure by growing the GNPs mass fraction. Li et al. [11] explored the nonlinear dynamic buckling and free vibration analyses of a sandwich plate with a porous core and two face sheets enriched with GNPs. They showed that subjoining GNPs dramatically improves the dynamic stability of like a plate. Wang et al. [12] explored the torsional buckling analysis of a GNP-reinforced cylindrical shell with a cut-out. It was observed by them that utilizing a higher number of layers reduces the stress gradient among the layers. The nonlinear dynamic analysis of a plate enriched with GNPs was examined by Gholami and Ansari [13]. They provided dynamic response curves to discover the relevance of the dynamic deflection on the dimensions and GNPs percentage. Safarpour et al. [14] demonstrated semi-analytical solutions for the vibration and static bending analyses of GNP-reinforced cylindrical and conical shells. They explored the relevance of the static deflection and the natural frequencies on the mass fraction and dispersion pattern of the GNPs. Incorporating temperature-dependent mechanical and thermal properties, Qaderi et al. [15] explored the free vibration behavior of a GNP-reinforced plate in a thermal environment. It was discovered by them that when a small amount of GNPs is added to the plate, the natural frequencies experience a considerable enhance. Saidi et al. [16] explored the aeroelastic stability analysis of a porous plate enriched with GNPs. It was observed by them that distributing more GNPs close to the surfaces of the plate brings about more expanded flutter boundaries.

The free vibration analysis of a cylindrical microshell enriched with GNPs was analyzed by Wang et al. [17]. They explored the relevance of the natural frequencies on the dimensions, mass fraction, and dispersion pattern of the GNPs. Wang et al. [18] explored the nonlinear vibration analysis of a metal foam cylindrical shell enriched by GNPs. It was shown that the mass fraction, dispersion pattern, and geometrical characteristics of the GNPs play significant roles in determining the nonlinear natural frequencies. Afshari [19,20] obtained the natural frequencies of spinning and non-rotating conical shells enriched with GNPs. It was observed by him that distributing the GNPs close to the inner surface of the shell brings about greater natural frequencies. Al-Furjan et al. [21] explored the low-velocity impact response of a sandwich truncated conical shell with a GNP-reinforced core and magnetostrictive face sheets. They discussed the impacts of the percentage and dispersion pattern of GNPs on the low-velocity impact properties of the shell. Arefi and Adab [22] examined the forced and free vibration and static bending analyses of a microplate enriched with GNPs. They discussed the impacts of the percentage and dispersion pattern of GNPs on the static and dynamic deflections and the natural frequencies of such a microplate. The aeroelastic stability characteristics of a laminated polymer/GNP/fiber composite conical-conical shell were explored by Nasution et al. [23]. Their results affirmed that growth in the GNPs mass fraction or glass fibers provides higher natural frequencies and more expanded flutter boundaries. Afshari and Adab [24] presented size-dependent analyses on the buckling and free vibrational behaviors of a thick microplate enriched with GNPs. They discovered that to raise the natural frequencies and buckling loads of such a structure, the square-shaped GNPs with fewer layers should be utilized. Adab et al. [25,26] examined the free vibration analysis of a conical shell in micro size including a porous core and two inner and outer layers enriched with GNPs. It was concluded by them that such a sandwich structure benefits from low weight and high stiffness. Fang et al. [27] examined the free vibration and thermal buckling characteristics of a rotating FG porous metal-matrix microplate enriched with GNPs. They examined the influences of rotation on the enriching effects of the GNPs. Sarafraz et al. [28,29] examined the free vibration, aeroelastic stability, and buckling analyses of a sandwich plate with an auxetic re-entrant honeycomb core and three-phase nanocomposite face sheets. They studied the relevance of the buckling loads, natural frequencies, and critical aerodynamic pressure of such a sandwich plate on the mass fractions of the GNPs and the fibers in the face sheets. Wang and Zhang [30] studied the temperature-dependent thermal buckling and postbuckling analyses of a porous nanocomposite beam enriched with GNPs. They investigated the temperature-relevance of mechanical and thermal properties on the thermal stability characteristics of such a beam. By considering temperature-dependent thermal and mechanical properties, Zhang et al. [31] explored the thermo-mechanical responses of porous FG GNP-reinforced cylindrical panels exposed to blast pressure. They focused on the impacts of the GNPs percentage and porosity parameters on the thermo-mechanical characteristics of such a panel.

Due to the low flexural rigidity of the nanofillers, the GNPs and CNTs tend to congregate together as a cluster which is called agglomeration. This inevitable phenomenon is not considered in the above-mentioned works. The relevance of the mechanical characteristics of nanocomposites enriched with CNTs on the CNTs agglomeration has been widely investigated by authors [32–41]. But there are few published papers related to the mechanical analysis of the structures reinforced with the agglomerated GNPs [42–45]. In the presented work, the forced and free vibration characteristics of thick plates enriched with GNPs are investigated by incorporating the GNPs agglomeration. The relevance of the natural frequencies and dynamic deflection on several parameters are explored and discussed such as the percentage and dispersion pattern of GNPs, and agglomeration parameters. Due to utilizing linear strain-displacement relations in the mathematical modeling of the plate and using the Navier method to provide an exact solution for the governing equations, the results of this work are limited to the free and forced vibration analyses of the simply supported plates with small deformations.

2. Geometry of the problem and effective mechanical properties

Based on Fig. 1, a rectangular plate exposed to the scattered load q is considered with geometrical properties including length b, width a, and uniform thickness h. The plate is enriched with GNPs which are dispersed within the polymeric matrix according to the various dispersion patterns depicted in Fig. 2 including the following patterns:

UD (uniform dispersion): In this pattern, the GNPs volume fraction is constant within the polymeric matrix.

FG-V: In this pattern, the GNPs volume fraction varies linearly from zero at the bottom surface to the maximum value at the top surface.

FG-O: In this pattern, the GNPs volume fraction varies linearly from zero at both surfaces to the maximum value at the middle surface.

FG-X: In this pattern, the GNPs volume fraction varies linearly from zero at the middle surface to the maximum value at both surfaces.

For these GNPs dispersion patterns, the GNPs volume fraction (F_r) is given below [24]:

$$\begin{aligned}
&UD: && F_r(z) = F_r^*,\\
&FG-V: && F_r(z) = F_r^*\left(1+2\frac{z}{h}\right),\\
&FG-O: && F_r(z) = 2F_r^*\left(1-2\frac{|z|}{h}\right),\\
&FG-X: && F_r(z) = 4F_r^*\frac{|z|}{h},
\end{aligned} \tag{1}$$

F_r^* is the total volume fraction of GNPs that is dependent on the GNPs mass fraction reinforcements (W_r) as [24]

$$F_r^* = \frac{W_r}{W_r + \frac{\rho_r}{\rho_m}(1-W_r)}, \tag{2}$$

where ρ stands for the density, the subscript r refers to the GNP reinforcements, and the subscript m stands for the matrix. Eq. (1) is regulated to bring about the same total GNPs volume fraction for all dispersion patterns to provide a fair comparison between them.

As described in the rule of mixture, the density of the plate is calculated as follows:

$$\rho = F_r\rho_r + F_m\rho_m, \tag{3}$$

where the volume fraction of the matrix is stated in the relation below:

$$F_m = 1 - F_r. \tag{4}$$

Due to the low flexural rigidity of the nanoparticles (CNTs and GNPs), they tend to cluster which is called agglomeration which attenuates the enriching effects of nanoparticles [46,47]. As can be seen in Fig. 1, a certain value of the GNPs appears in the cluster form and the other GNPs scatter within the polymeric matrix. For this case, the equivalent elastic constants such as elastic, bulk, and shear moduli, and Poisson's ratio can be estimated via the Eshelby-Mori-Tanaka approach [48,49]. To incorporate the influence of the GNPs agglomeration in the presented model, a two-parameter model presented by Shi et al. [50] is hired. As stated in this model, the GNPs agglomeration is expressed utilizing the following dimensionless parameters:

$$\mu = \frac{V_{cluster}}{V}, \quad \eta = \frac{V_r^{in}}{V_r}, \tag{5}$$

in which V refers to the volume of the plate, $V_{cluster}$ stands for the volume of the clusters, V_r represents the volume of the GNP reinforcements, and V_r^{in} indicates the volume of agglomerated GNPs.

For an isotropic material, the Poisson's ratio (ν) and the elastic modulus (E) are demonstrated in terms of bulk (K) and shear (G)

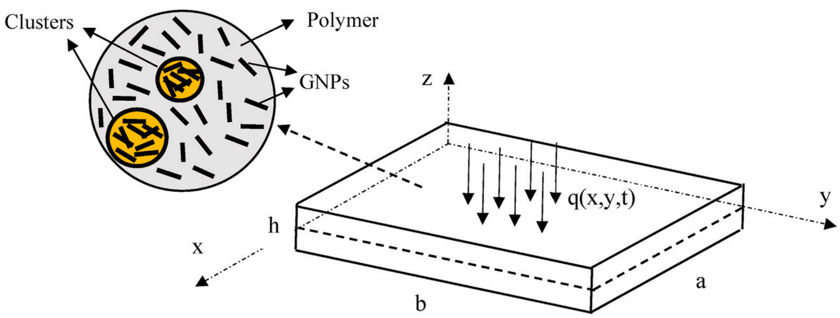

Fig. 1. A rectangular thick plate reinforced with agglomerated GNPs.

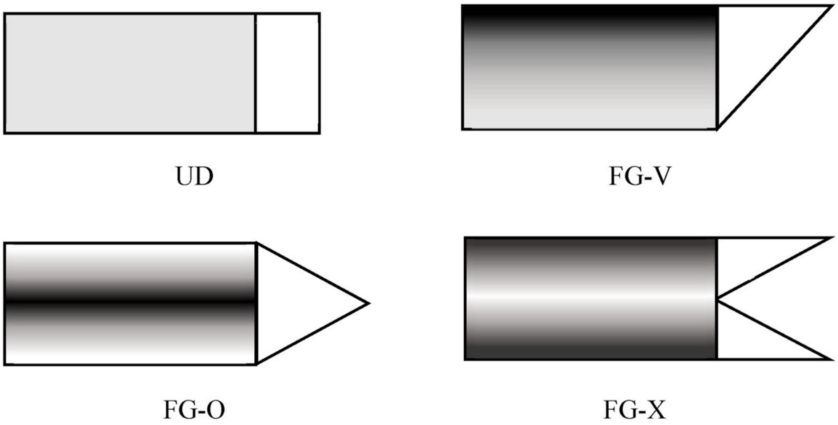

Fig. 2. GNPs dispersion patterns.

moduli as the relations which is demonstrated:

$$\nu = \frac{3K - 2G}{6K + 2G}, \quad E = \frac{9KG}{3K + G}, \tag{6}$$

in which bulk and shear are computed as follows [42]:

$$K = K_{out}\left[1 + \frac{\mu\left(\frac{K_{in}}{K_{out}} - 1\right)}{1 + \frac{1-\mu}{3}\frac{1+\nu_{out}}{1-\nu_{out}}\left(\frac{K_{in}}{K_{out}} - 1\right)}\right], \quad G = G_{out}\left[1 + \frac{\mu\left(\frac{G_{in}}{G_{out}} - 1\right)}{1 + \frac{2(1-\mu)}{15}\frac{4-5\nu_{out}}{1-\nu_{out}}\left(\frac{G_{in}}{G_{out}} - 1\right)}\right], \tag{7}$$

where the subscripts “out” and “in” sequentially describe the outside and inside of the clusters and [42].

$$\begin{aligned}
&\nu_{out} = \frac{3K_{out} - 2G_{out}}{6K_{out} + 2G_{out}}, \quad K_{in} = K_m + \frac{F_r\eta(\delta_r - 3K_m\alpha_r)}{3[\mu + \eta(\alpha_r - 1)F_r]}, \quad G_{in} = G_m + \frac{F_r\eta(\eta_r - 2G_m\beta_r)}{2[\mu + \eta(\beta_r - 1)F_r]}, \\
&K_{out} = K_m + \frac{F_r(1-\eta)(\delta_r - 3K_m\alpha_r)}{3[1 - \mu + (\alpha_r - 1)(1-\eta)F_r]}, \quad G_{out} = G_m + \frac{F_r(1-\eta)(\eta_r - 2G_m\beta_r)}{2[1 - \mu + (\beta_r - 1)(1-\eta)F_r]},
\end{aligned} \tag{8}$$

in which the bulk and shear moduli of the polymeric matrix are presented as follows:

$$K_m = \frac{E_m}{3 - 6\nu_m}, \quad G_m = \frac{E_m}{2 + 2\nu_m}, \tag{9}$$

in which [42].

$$\begin{aligned}
&\alpha_r = \frac{3K_m + 2n_r - 2l_r}{3n_r}, \quad \beta_r = \frac{4G_m + 7n_r + 2l_r}{15n_r} - \frac{2G_m}{5p_r}, \\
&\eta_r = \frac{2}{15}\left(k_r + 6m_r + 8G_m - \frac{l_r^2 + 2G_m l_r}{n_r}\right), \quad \delta_r = \frac{3K_m(n_r + 2l_r) + 4\left(k_r n_r - l_r^2\right)}{3n_r},
\end{aligned} \tag{10}$$

where the five constants (p_r, n_r, m_r, l_r, k_r) are called Hill’s elastic moduli. These constants are related to the GNPs and are presented in Table 1 along with the density of the GNPs.

3. Displacement, strain, and stress

As a common basic assumption in the classical plate theory (CPT), the first-order and third-order shear deformation theories (FSDT and TSDT), and other higher-order shear deformation theories, it is supposed that the thickness of the plate remains constant during deformation. This assumption is acceptable for thin to moderately thick plates but brings about low precision for thick plates. To improve the precision of the model for hick plates, quasi-3D shear deformation theories have been proposed in recent years. In such

Table 1
Mechanical properties of the GNPs [3,42].

p_r	n_r	m_r	l_r	k_r	ρ_r
102000 GPa	102000 GPa	369 GPa	6.8 GPa	850 GPa	1060 kg/m^3

plate theories, the thickness stretching is incorporated along with shear deformations which improves the precision of the results, especially for thick plates.

As stated the in the quasi-3D HSDT, the displacement field can be considered as follows [51]:

$$\begin{Bmatrix} u_1(t,z,y,x) \\ u_2(t,z,y,x) \end{Bmatrix} = \begin{Bmatrix} u(t,y,x) \\ v(t,y,x) \end{Bmatrix} - z\begin{Bmatrix} \dfrac{\partial w_b}{\partial x} \\ \dfrac{\partial w_b}{\partial y} \end{Bmatrix} - \psi(z)\begin{Bmatrix} \dfrac{\partial w_s}{\partial x} \\ \dfrac{\partial w_s}{\partial y} \end{Bmatrix}, \quad u_3(t,z,y,x) = w_s(t,y,x) + w_b(t,y,x) + s(z)\varphi_z(t,y,x), \tag{11}$$

u_1, u_2, and u_3 sequentially refer to the components of displacement along x, y, and z directions, u, v, φ_z, w_s, and w_b are unknown functions, and the relations below are presented for functions $\psi(z)$ and $s(z)$:

$$\psi(z) = h\left\{\left[1+\cosh\left(\frac{1}{2}\right)\right]\frac{z}{h} - \sinh\left(\frac{z}{h}\right)\right\}, \quad s(z) = 1 - \frac{d\psi}{dz} = \cosh\left(\frac{z}{h}\right) - \cosh\left(\frac{1}{2}\right). \tag{12}$$

The components of strain are presented as the relations below:

$$\begin{aligned} &\varepsilon_x = \frac{\partial u_1}{\partial x} = \frac{\partial u}{\partial x} - z\frac{\partial^2 w_b}{\partial x^2} - \psi\frac{\partial^2 w_s}{\partial x^2}, \quad \varepsilon_y = \frac{\partial u_2}{\partial y} = \frac{\partial v}{\partial y} - z\frac{\partial^2 w_b}{\partial y^2} - \psi\frac{\partial^2 w_s}{\partial y^2}, \\ &\varepsilon_z = \frac{\partial u_3}{\partial z} = \frac{ds}{dz}\varphi_z, \quad \gamma_{yz} = \frac{\partial u_2}{\partial z} + \frac{\partial u_3}{\partial y} = s\left(\frac{\partial w_s}{\partial y} + \frac{\partial \varphi_z}{\partial y}\right), \\ &\gamma_{xz} = \frac{\partial u_1}{\partial z} + \frac{\partial u_3}{\partial x} = s\left(\frac{\partial w_s}{\partial x} + \frac{\partial \varphi_z}{\partial x}\right), \quad \gamma_{xy} = \frac{\partial u_1}{\partial y} + \frac{\partial u_2}{\partial x} = \frac{\partial u}{\partial y} + \frac{\partial v}{\partial x} - 2z\frac{\partial^2 w_b}{\partial x \partial y} - 2\psi\frac{\partial^2 w_s}{\partial x \partial y}, \end{aligned} \tag{13}$$

and the stress tensor can be stated as

$$\begin{Bmatrix} \sigma_x \\ \sigma_y \\ \sigma_z \\ \sigma_{yz} \\ \sigma_{xz} \\ \sigma_{xy} \end{Bmatrix} = \begin{bmatrix} C_{11} & C_{12} & C_{13} & 0 & 0 & 0 \\ C_{12} & C_{22} & C_{23} & 0 & 0 & 0 \\ C_{13} & C_{23} & C_{33} & 0 & 0 & 0 \\ 0 & 0 & 0 & C_{44} & 0 & 0 \\ 0 & 0 & 0 & 0 & C_{55} & 0 \\ 0 & 0 & 0 & 0 & 0 & C_{66} \end{bmatrix} \begin{Bmatrix} \varepsilon_x \\ \varepsilon_y \\ \varepsilon_z \\ \gamma_{yz} \\ \gamma_{xz} \\ \gamma_{xy} \end{Bmatrix}, \tag{14}$$

where

$$C_{ij} = \begin{cases} \dfrac{1-\nu}{1+\nu}\dfrac{0.5E}{0.5-\nu}, & i=j=1,2,3. \\ \dfrac{0.5E}{1+\nu}, & i=j=4,5,6. \\ \dfrac{\nu}{1+\nu}\dfrac{0.5E}{0.5-\nu}, & i \neq j. \end{cases} \tag{15}$$

As observed in Eq. (13), $\varepsilon_{zz} \neq 0$ which indicates the thickness stretching in the quasi-3D HSDT.

4. Governing equations

The governing equations can be obtained utilizing the following relation called Hamilton's principle:

$$\int_{t_1}^{t_2} (\delta W + \delta T - \delta U)dt = 0 \tag{16}$$

where T refers to kinematic energy, U represents strain energy, and W means the work done by non-conservative loads. δ denotes the well-known variational operator, and t_1 and t_2 are two arbitrary moments.

The following equation presents the strain energy:

$$U = 0.5\iiint_V \left(\varepsilon_x\sigma_x + \varepsilon_y\sigma_y + \varepsilon_z\sigma_z + \gamma_{xy}\sigma_{xy} + \gamma_{xz}\sigma_{xz} + \gamma_{yz}\sigma_{yz}\right)dV, \tag{17}$$

which brings about the following relation of the variation of the strain energy:

$$\delta U = \iiint_V \left(\delta\varepsilon_x\sigma_x + \delta\varepsilon_y\sigma_y + \delta\varepsilon_z\sigma_z + \delta\gamma_{xy}\sigma_{xy} + \delta\gamma_{xz}\sigma_{xz} + \delta\gamma_{yz}\sigma_{yz}\right)dV, \tag{18}$$

and

$$\iiint_V ()dV = \iint_S \int_{-\frac{h}{2}}^{\frac{h}{2}} ()dzdS, \tag{19}$$

in which S refers to the area of the plate in the x-y plane ($dS = dxdy$).
Based on Eqs. (13) and (19), Eq. (18) can be represented in the relation below:

$$\begin{aligned}\delta U = \iint_S \Bigg(& N_x\frac{\partial \delta u}{\partial x} - M_x\frac{\partial^2 \delta w_b}{\partial x^2} - P_x\frac{\partial^2 \delta w_s}{\partial x^2} + N_y\frac{\partial \delta v}{\partial y} - M_y\frac{\partial^2 \delta w_b}{\partial y^2} - P_y\frac{\partial^2 \delta w_s}{\partial y^2} + R_z\delta\varphi_z + N_{xy}\frac{\partial \delta u}{\partial y} \\ & + N_{xy}\frac{\partial \delta v}{\partial x} - 2M_{xy}\frac{\partial^2 \delta w_b}{\partial x\partial y} - 2P_{xy}\frac{\partial^2 \delta w_s}{\partial x\partial y} + Q_{xz}\frac{\partial \delta w_s}{\partial x} + Q_{xz}\frac{\partial \delta \varphi_z}{\partial x} + Q_{yz}\frac{\partial \delta w_s}{\partial y} + Q_{yz}\frac{\partial \delta \varphi_z}{\partial y}\Bigg)dS,\end{aligned} \tag{20}$$

where

$$\begin{aligned}&\begin{Bmatrix} N_x \\ N_y \\ N_{xy}\end{Bmatrix} = \int_{-\frac{h}{2}}^{\frac{h}{2}} \begin{Bmatrix} \sigma_x \\ \sigma_y \\ \sigma_{xy}\end{Bmatrix} dz, \quad \begin{Bmatrix} M_x \\ M_y \\ M_{xy}\end{Bmatrix} = \int_{-\frac{h}{2}}^{\frac{h}{2}} z\begin{Bmatrix} \sigma_x \\ \sigma_y \\ \sigma_{xy}\end{Bmatrix} dz, \quad \begin{Bmatrix} P_x \\ P_y \\ P_{xy}\end{Bmatrix} = \int_{-\frac{h}{2}}^{\frac{h}{2}} \psi(z)\begin{Bmatrix} \sigma_x \\ \sigma_y \\ \sigma_{xy}\end{Bmatrix} dz, \\ &\begin{Bmatrix} Q_{xz} \\ Q_{yz}\end{Bmatrix} = \int_{-\frac{h}{2}}^{\frac{h}{2}} g(z)\begin{Bmatrix} \sigma_{xz} \\ \sigma_{yz}\end{Bmatrix} dz, \quad R_z = \int_{-\frac{h}{2}}^{\frac{h}{2}} \frac{dg(z)}{dz}\sigma_z dz.\end{aligned} \tag{21}$$

In conjunction with Eqs. (13) and (14), Eq. (21) can be represented as below:

$$\begin{aligned}
N_x &= A_1\frac{\partial u}{\partial x} - A_2\frac{\partial^2 w_b}{\partial x^2} - A_3\frac{\partial^2 w_s}{\partial x^2} + B_1\frac{\partial v}{\partial y} - B_2\frac{\partial^2 w_b}{\partial y^2} - B_3\frac{\partial^2 w_s}{\partial y^2} + D_1\varphi_z, \\
N_y &= B_1\frac{\partial u}{\partial x} - B_2\frac{\partial^2 w_b}{\partial x^2} - B_3\frac{\partial^2 w_s}{\partial x^2} + G_1\frac{\partial v}{\partial y} - G_2\frac{\partial^2 w_b}{\partial y^2} - G_3\frac{\partial^2 w_s}{\partial y^2} + J_1\varphi_z, \\
N_{xy} &= H_1\frac{\partial u}{\partial y} + H_1\frac{\partial v}{\partial x} - 2H_2\frac{\partial^2 w_b}{\partial x\partial y} - 2H_3\frac{\partial^2 w_s}{\partial x\partial y}, \\
M_x &= A_2\frac{\partial u}{\partial x} - A_4\frac{\partial^2 w_b}{\partial x^2} - A_5\frac{\partial^2 w_s}{\partial x^2} + B_2\frac{\partial v}{\partial y} - B_4\frac{\partial^2 w_b}{\partial y^2} - B_5\frac{\partial^2 w_s}{\partial y^2} + D_2\varphi_z, \\
M_y &= B_2\frac{\partial u}{\partial x} - B_4\frac{\partial^2 w_b}{\partial x^2} - B_5\frac{\partial^2 w_s}{\partial x^2} + G_2\frac{\partial v}{\partial y} - G_4\frac{\partial^2 w_b}{\partial y^2} - G_5\frac{\partial^2 w_s}{\partial y^2} + J_2\varphi_z, \\
M_{xy} &= H_2\frac{\partial u}{\partial y} + H_2\frac{\partial v}{\partial x} - 2H_4\frac{\partial^2 w_b}{\partial x\partial y} - 2H_5\frac{\partial^2 w_s}{\partial x\partial y}, \\
P_x &= A_3\frac{\partial u}{\partial x} - A_5\frac{\partial^2 w_b}{\partial x^2} - A_6\frac{\partial^2 w_s}{\partial x^2} + B_3\frac{\partial v}{\partial y} - B_5\frac{\partial^2 w_b}{\partial y^2} - B_6\frac{\partial^2 w_s}{\partial y^2} + D_3\varphi_z, \\
P_y &= B_3\frac{\partial u}{\partial x} - B_5\frac{\partial^2 w_b}{\partial x^2} - B_6\frac{\partial^2 w_s}{\partial x^2} + G_3\frac{\partial v}{\partial y} - G_5\frac{\partial^2 w_b}{\partial y^2} - G_6\frac{\partial^2 w_s}{\partial y^2} + J_3\varphi_z, \\
P_{xy} &= H_3\frac{\partial u}{\partial y} + H_3\frac{\partial v}{\partial x} - 2H_5\frac{\partial^2 w_b}{\partial x\partial y} - 2H_6\frac{\partial^2 w_s}{\partial x\partial y}, \\
Q_{xz} &= K_2\left(\frac{\partial w_s}{\partial x} + \frac{\partial \varphi_z}{\partial x}\right), \quad Q_{yz} = K_1\left(\frac{\partial w_s}{\partial y} + \frac{\partial \varphi_z}{\partial y}\right), \\
R_z &= D_1\frac{\partial u}{\partial x} - D_2\frac{\partial^2 w_b}{\partial x^2} - D_3\frac{\partial^2 w_s}{\partial x^2} + J_1\frac{\partial v}{\partial y} - J_2\frac{\partial^2 w_b}{\partial y^2} - J_3\frac{\partial^2 w_s}{\partial y^2} + L_1\varphi_z,
\end{aligned} \tag{22}$$

in which

$$\begin{Bmatrix} A_1 \\ A_2 \\ A_3 \\ A_4 \\ A_5 \\ A_6 \end{Bmatrix} = \int_{-\frac{h}{2}}^{\frac{h}{2}} C_{11}(z) \begin{Bmatrix} 1 \\ z \\ \psi(z) \\ z^2 \\ z\psi(z) \\ \psi^2(z) \end{Bmatrix} dz, \quad \begin{Bmatrix} B_1 \\ B_2 \\ B_3 \\ B_4 \\ B_5 \\ B_6 \end{Bmatrix} = \int_{-\frac{h}{2}}^{\frac{h}{2}} C_{12}(z) \begin{Bmatrix} 1 \\ z \\ \psi(z) \\ z^2 \\ z\psi(z) \\ \psi^2(z) \end{Bmatrix} dz,$$

$$\begin{Bmatrix} G_1 \\ G_2 \\ G_3 \\ G_4 \\ G_5 \\ G_6 \end{Bmatrix} = \int_{-\frac{h}{2}}^{\frac{h}{2}} C_{22}(z) \begin{Bmatrix} 1 \\ z \\ \psi(z) \\ z^2 \\ z\psi(z) \\ \psi^2(z) \end{Bmatrix} dz, \quad \begin{Bmatrix} H_1 \\ H_2 \\ H_3 \\ H_4 \\ H_5 \\ H_6 \end{Bmatrix} = \int_{-\frac{h}{2}}^{\frac{h}{2}} C_{66}(z) \begin{Bmatrix} 1 \\ z \\ \psi(z) \\ z^2 \\ z\psi(z) \\ \psi^2(z) \end{Bmatrix} dz, \tag{23}$$

$$\begin{Bmatrix} D_1 \\ D_2 \\ D_3 \end{Bmatrix} = \int_{-\frac{h}{2}}^{\frac{h}{2}} C_{13}(z) \frac{ds}{dz} \begin{Bmatrix} 1 \\ z \\ \psi(z) \end{Bmatrix} dz, \quad \begin{Bmatrix} J_1 \\ J_2 \\ J_3 \end{Bmatrix} = \int_{-\frac{h}{2}}^{\frac{h}{2}} C_{23}(z) \frac{ds}{dz} \begin{Bmatrix} 1 \\ z \\ \psi(z) \end{Bmatrix} dz,$$

$$\begin{Bmatrix} K_1 \\ K_2 \end{Bmatrix} = \int_{-\frac{h}{2}}^{\frac{h}{2}} \begin{Bmatrix} C_{44}(z) \\ C_{55}(z) \end{Bmatrix} s^2(z) dz, \quad L_1 = \int_{-\frac{h}{2}}^{\frac{h}{2}} C_{33}(z) \left(\frac{ds}{dz}\right)^2 dz.$$

The following equation provides the kinetic energy:

$$T = 0.5 \iiint_V \rho \left[\left(\frac{\partial u_1}{\partial t}\right)^2 + \left(\frac{\partial u_2}{\partial t}\right)^2 + \left(\frac{\partial u_3}{\partial t}\right)^2 \right] dV, \tag{24}$$

which brings about the following relation:

$$\delta T = \iiint_V \rho \left(\frac{\partial u_1}{\partial t} \frac{\partial \delta u_1}{\partial t} + \frac{\partial u_2}{\partial t} \frac{\partial \delta u_2}{\partial t} + \frac{\partial u_3}{\partial t} \frac{\partial \delta u_3}{\partial t} \right) dV. \tag{25}$$

By considering Eqs. (11) and (19), the relation below is achieved:

$$\begin{aligned} \delta T = \iint_S \Big(& I_0 \frac{\partial u}{\partial t} \frac{\partial \delta u}{\partial t} + I_2 \frac{\partial^2 w_b}{\partial t \partial x} \frac{\partial^2 \delta w_b}{\partial t \partial x} + I_5 \frac{\partial^2 w_s}{\partial t \partial x} \frac{\partial^2 \delta w_s}{\partial t \partial x} - I_1 \frac{\partial \delta u}{\partial t} \frac{\partial^2 w_b}{\partial t \partial x} - I_1 \frac{\partial u}{\partial t} \frac{\partial^2 \delta w_b}{\partial t \partial x} - I_3 \frac{\partial \delta u}{\partial t} \frac{\partial^2 w_s}{\partial t \partial x} - I_3 \frac{\partial u}{\partial t} \frac{\partial^2 \delta w_s}{\partial t \partial x} + I_4 \frac{\partial^2 \delta w_b}{\partial t \partial x} \frac{\partial^2 w_s}{\partial t \partial x} \\ & + I_4 \frac{\partial^2 w_b}{\partial t \partial x} \frac{\partial^2 \delta w_s}{\partial t \partial x} + I_0 \frac{\partial v}{\partial t} \frac{\partial \delta v}{\partial t} + I_2 \frac{\partial^2 w_b}{\partial t \partial y} \frac{\partial^2 \delta w_b}{\partial t \partial y} + I_5 \frac{\partial^2 w_s}{\partial t \partial y} \frac{\partial^2 \delta w_s}{\partial t \partial y} - I_1 \frac{\partial \delta v}{\partial t} \frac{\partial^2 w_b}{\partial t \partial y} - I_1 \frac{\partial v}{\partial t} \frac{\partial^2 \delta w_b}{\partial t \partial y} - I_3 \frac{\partial \delta v}{\partial t} \frac{\partial^2 w_s}{\partial t \partial y} - I_3 \frac{\partial v}{\partial t} \frac{\partial^2 \delta w_s}{\partial t \partial y} \\ & + I_4 \frac{\partial^2 \delta w_b}{\partial t \partial y} \frac{\partial^2 w_s}{\partial t \partial y} + I_4 \frac{\partial^2 w_b}{\partial t \partial y} \frac{\partial^2 \delta w_s}{\partial t \partial y} + I_0 \frac{\partial w_b}{\partial t} \frac{\partial \delta w_b}{\partial t} + I_0 \frac{\partial w_s}{\partial t} \frac{\partial \delta w_s}{\partial t} + I_7 \frac{\partial \varphi_z}{\partial t} \frac{\partial \delta \varphi_z}{\partial t} \\ & + I_0 \frac{\partial \delta w_b}{\partial t} \frac{\partial w_s}{\partial t} + I_0 \frac{\partial w_b}{\partial t} \frac{\partial \delta w_s}{\partial t} + I_6 \frac{\partial \delta w_b}{\partial t} \frac{\partial \varphi_z}{\partial t} + I_6 \frac{\partial w_b}{\partial t} \frac{\partial \delta \varphi_z}{\partial t} + I_6 \frac{\partial \delta w_s}{\partial t} \frac{\partial \varphi_z}{\partial t} + I_6 \frac{\partial w_s}{\partial t} \frac{\partial \delta \varphi_z}{\partial t} \Big) dS, \end{aligned} \tag{26}$$

where

$$\begin{Bmatrix} I_0 \\ I_1 \\ I_2 \\ I_3 \\ I_4 \\ I_5 \\ I_6 \\ I_7 \end{Bmatrix} = \int_{-\frac{h}{2}}^{\frac{h}{2}} \rho(z) \begin{Bmatrix} 1 \\ z \\ z^2 \\ \psi(z) \\ z\psi(z) \\ \psi^2(z) \\ s(z) \\ s^2(z) \end{Bmatrix} dz, \tag{27}$$

The following relation shows the study carried out by non-conservative external load q scattered on the top surface of the plate:

$$W = \iint_S q(x,y,t)u_3|_{z=\frac{h}{2}} dS = \iint_S q(x,y,t)(w_b + w_s)dS, \tag{28}$$

which brings about the following relation:

$$\delta W = \iint_S q(x,y,t)(\delta w_b + \delta w_s)dS. \tag{29}$$

Substituting Eqs. (20), (26) and (29) into Eq. (16) brings about the relations below as the governing equations:

$$\begin{aligned}
&-I_0\frac{\partial^2 u}{\partial t^2} + I_1\frac{\partial^3 w_b}{\partial t^2 \partial x} + I_3\frac{\partial^3 w_s}{\partial t^2 \partial x} + \frac{\partial N_x}{\partial x} + \frac{\partial N_{xy}}{\partial y} = 0, \\
&-I_0\frac{\partial^2 v}{\partial t^2} + I_1\frac{\partial^3 w_b}{\partial t^2 \partial y} + I_3\frac{\partial^3 w_s}{\partial t^2 \partial y} + \frac{\partial N_y}{\partial y} + \frac{\partial N_{xy}}{\partial x} = 0, \\
&-I_1\frac{\partial^3 u}{\partial t^2 \partial x} - I_1\frac{\partial^3 v}{\partial t^2 \partial y} + I_2\frac{\partial^4 w_b}{\partial t^2 \partial x^2} + I_2\frac{\partial^4 w_b}{\partial t^2 \partial y^2} - I_0\frac{\partial^2 w_b}{\partial t^2} + I_4\frac{\partial^4 w_s}{\partial t^2 \partial x^2} \\
&+I_4\frac{\partial^4 w_s}{\partial t^2 \partial y^2} - I_0\frac{\partial^2 w_s}{\partial t^2} - I_6\frac{\partial^2 \varphi_z}{\partial t^2} + \frac{\partial^2 M_x}{\partial x^2} + \frac{\partial^2 M_y}{\partial y^2} + 2\frac{\partial^2 M_{xy}}{\partial x \partial y} = -q, \\
&-I_3\frac{\partial^3 u}{\partial t^2 \partial x} - I_3\frac{\partial^3 v}{\partial t^2 \partial y} + I_4\frac{\partial^4 w_b}{\partial t^2 \partial x^2} + I_4\frac{\partial^4 w_b}{\partial t^2 \partial y^2} - I_0\frac{\partial^2 w_b}{\partial t^2} + I_5\frac{\partial^4 w_s}{\partial t^2 \partial x^2} + I_5\frac{\partial^4 w_s}{\partial t^2 \partial y^2} \\
&-I_0\frac{\partial^2 w_s}{\partial t^2} - I_6\frac{\partial^2 \varphi_z}{\partial t^2} + \frac{\partial^2 P_x}{\partial x^2} + \frac{\partial^2 P_y}{\partial y^2} + 2\frac{\partial^2 P_{xy}}{\partial x \partial y} + \frac{\partial Q_{xz}}{\partial x} + \frac{\partial Q_{yz}}{\partial y} = -q, \\
&-I_6\frac{\partial^2 w_b}{\partial t^2} - I_6\frac{\partial^2 w_s}{\partial t^2} - I_7\frac{\partial^2 \varphi_z}{\partial t^2} - R_z + \frac{\partial Q_{xz}}{\partial x} + \frac{\partial Q_{yz}}{\partial y} = 0,
\end{aligned} \tag{30}$$

5. Solution

An exaction solution is performed here for the governing equation (30) utilizing the Navier method. By substituting Eq. (22) into Eq. (30), selecting the following series-based solution for a simply supported plate:

$$\begin{aligned}
u(t,y,x) &= \sum_{n=1}^{\infty}\sum_{m=1}^{\infty}\sin(\beta y)\cos(\alpha x)U_{mn}(t), \\
v(t,y,x) &= \sum_{n=1}^{\infty}\sum_{m=1}^{\infty}\cos(\beta y)\sin(\alpha x)V_{mn}(t),
\end{aligned}
\quad
\begin{Bmatrix} w_b(t,y,x) \\ w_s(t,y,x) \\ \varphi_z(t,y,x) \end{Bmatrix} = \sum_{n=1}^{\infty}\sum_{m=1}^{\infty}\sin(\beta y)\sin(\alpha x)\begin{Bmatrix} W_{bmn}(t) \\ W_{smn}(t) \\ \varphi_{zmn}(t) \end{Bmatrix}, \tag{31}$$

in which

$$\alpha = \frac{m\pi}{a}, \quad \beta = \frac{n\pi}{b}, \tag{32}$$

and considering the following Fourier sinusoidal expansion for the external load q:

$$q(t,y,x) = \sum_{n=1}^{\infty}\sum_{m=1}^{\infty}\sin(\beta y)\sin(\alpha x)q_{mn}(t), \tag{33}$$

in which

$$q_{mn}(t) = \frac{4}{ab}\int_0^a\int_0^b \sin(\beta y)\sin(\alpha x)q(t,x,y)dxdy, \tag{34}$$

The following equation can be achieved:

$$[M]\left\{\frac{d^2 s}{dt^2}\right\} + [K]\{s\} = \{f(t)\}, \tag{35}$$

where

$$\{s\} = \begin{Bmatrix} U_{mn} \\ V_{mn} \\ W_{bmn} \\ W_{smn} \\ \varphi_{zmn} \end{Bmatrix}, \quad \{f\} = \begin{Bmatrix} 0 \\ 0 \\ -q_{mn} \\ -q_{mn} \\ 0 \end{Bmatrix}, \tag{36}$$

and $K_{ij} = K_{ji}$ and $M_{ij} = M_{ji}$ are defined as follows:

$$\begin{aligned}
&M_{11} = -I_0, \quad M_{22} = -I_0, \quad M_{34} = -\left[I_0 + I_4\left(\alpha^2 + \beta^2\right)\right],\\
&M_{12} = 0, \quad M_{23} = I_1\beta, \quad M_{35} = -I_6,\\
&M_{13} = I_1\alpha, \quad M_{24} = I_3\beta, \quad M_{44} = -\left[I_0 + I_5\left(\alpha^2 + \beta^2\right)\right],\\
&M_{14} = I_3\alpha, \quad M_{25} = 0, \quad M_{45} = -I_6,\\
&M_{15} = 0, \quad M_{33} = -\left[I_0 + I_2\left(\alpha^2 + \beta^2\right)\right], \quad M_{55} = -I_7,\\
&K_{11} = -A_1\alpha^2 - H_1\beta^2, \quad K_{12} = -B_1\alpha\beta - H_1\alpha\beta, \quad K_{13} = A_2\alpha^3 + B_2\alpha\beta^2 + 2H_2\alpha\beta^2,\\
&K_{14} = A_3\alpha^3 + B_3\alpha\beta^2 + 2H_3\alpha\beta^2, \quad K_{15} = D_1\alpha, \quad K_{22} = -G_1\beta^2 - H_1\alpha^2,\\
&K_{23} = B_2\alpha^2\beta + G_2\beta^3 + 2H_2\alpha^2\beta, \quad K_{24} = B_3\alpha^2\beta + G_3\beta^3 + 2H_3\alpha^2\beta, \quad K_{25} = J_1\beta,\\
&K_{33} = -\left[A_4\alpha^4 + 2(B_4 + 2H_4)\alpha^2\beta^2 + G_4\beta^4\right], \quad K_{34} = -\left[A_5\alpha^4 + 2(B_5 + 2H_5)\alpha^2\beta^2 + G_5\beta^4\right],\\
&K_{35} = -\left(D_2\alpha^2 + J_2\beta^2\right), \quad K_{44} = -\left[A_6\alpha^4 + 2(B_6 + 2H_6)\alpha^2\beta^2 + K_2\alpha^2 + G_6\beta^4 + K_1\beta^2\right],\\
&K_{45} = -\left[(D_3 + K_2)\alpha^2 + (J_3 + K_1)\beta^2\right], \quad K_{55} = -\left(K_2\alpha^2 + K_1\beta^2 + L_1\right),
\end{aligned} \tag{37}$$

In the forced vibration study of the rectangular plate exposed to an arbitrary external load q, Eq. (35) is solved approximately via the Newmark method [52]. In the free vibration analysis, by considering $q = 0$ (which brings about $f = 0$), and selecting the following solution:

$$\{s(t)\} = \{s_0\}e^{i\omega t}, \tag{38}$$

ω refers to the natural frequency, one can find the eigenvalue equation below:

$$[K]\{s_0\} = \omega^2[M]\{s_0\}. \tag{39}$$

For each pair of m and n, the solution of the eigenvalue equation (39) brings about the natural frequencies (ω_{mn}).

6. Numerical investigations and discussions

Numerical finding are demonstrated and discussed here to discover the impacts of different parameters on the dynamic characteristics of the plate including the dynamic deflection and the natural frequencies.

Other than the cases specifically mentioned, a rectangular plate of $h = 10$ cm, $a/h = 10$, and $b/h = 20$ is chosen. Epoxy ($\rho_m = 1200$ kg/m^3, $E_m = 3$ GPa, $\nu_m = 0.34$) is selected as the matrix which is reinforced with GNPs (check Table 1) with $W_r = 0.01$, scattered according to the FG-X dispersion pattern, with the agglomeration parameters (η,μ)=(0.8,0.2). In the forced vibration analysis, a concentrated load as $q = 10^6\exp(-0.2t)\sin(t)$ N is utilized on the center point of the plate (x_q,y_q)=(a/2,b/2). The dimensionless forms of the dynamic deflection and the natural frequencies are defined as follows:

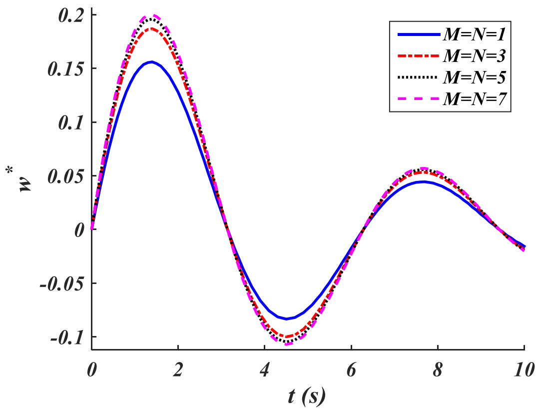

Fig. 3. Convergence analysis.

$$\lambda_{mn} = \omega_{mn} a \sqrt{\frac{\rho_m}{E_m}}, \quad w^* = \frac{1}{h} w\left(\frac{a}{2}, \frac{b}{2}, t\right). \tag{40}$$

It is noteworthy that in the forced vibration analysis, the parameters in the solution provided via the Newmark method are chosen to make it stable for any values of the time step [52]. To provide accurate results, the time step is considered as $\Delta t = 0.1\ s$ and the solution is performed for $0 \leq t \leq 10\ s$. Also, the initial conditions (the deformation and velocity of the plate at the time that the load q is applied) are considered zero.

6.1. Convergence

In practice, the truncated series in the Navier solution (Eq. (31) and (33)) should be employed ($m = 1,2,3, \ldots, M$ and $n = 1,2,3, \ldots, N$). To determine the required values of M and N, the dimensionless dynamic deflection of the plate is shown in Fig. 3 for $M = N = 1,3,5,7$. As demonstarted, the employed Navier solution converges quickly and hereafter the dimensionless dynamic deflection is reported for $M = N = 5$.

6.2. Verification

To investigate the precision and verification of the presented model, assume a square plate of $h/a = 0.1$ and $b = a = 0.45$ m enriched with GNPs. By neglecting the GNPs agglomeration ($\mu = \eta = 1$), Poisson's ratio is predicted using the rule of mixture as the relation below:

$$\nu = F_r \nu_r + F_m \nu_m, \tag{41}$$

in which $\nu_r = 0.186$ refers to Poisson's ratio of the GNP reinforcements. The elastic modulus is estimated via Halpin-Tsai as the relation below [53]:

$$E = \left[\frac{3(1 + \xi_L \eta_L F_r)}{1 - \eta_L F_r} + \frac{5(1 + \xi_w \eta_w F_r)}{1 - \eta_w F_r}\right] \frac{E_m}{8}, \tag{42}$$

in which

$$\xi_L = \frac{2l_r}{h_r}, \quad \xi_w = \frac{2w_r}{h_r}, \quad \eta_L = \frac{\eta - 1}{\eta + \xi_L}, \quad \eta_w = \frac{\eta - 1}{\eta + \xi_w}, \quad \eta = \frac{E_r}{E_m}, \tag{43}$$

in which $E_r = 1010$ GPa refers to the elastic modulus of the GNP reinforcements and $h_r = 1.5$ nm, $w_r = 1.5$ μm, and $l_r = 2.5$ μm sequentially indicate the thickness, width, and length of the GNPs. For different dispersion patterns of the GNPs and some selected vibrational modes, the dimensionless frequency parameters are listed in Table 2 alongside those demonstrated by Song et al. [7] and Afshari and Adab [24]. The results presented in Table 2 are in an acceptable agreement that affirms the precision of the introduced model. It is noteworthy that the small discrepancy between the results reported in Ref. [7] and those obtained in the presented work and Ref. [24] is generated by the differences between the used plate theories. In Ref. [7], the FSDT is utilized, but more accurate theories are employed in the current work and Ref. [24] which respectively are the quasi-3D HSDT and the quasi-3D sinusoidal shear deformation theory (quasi-3D SSDT).

Table 2 shows that for UD and FG-V, the natural frequencies presented in Ref. [7] are lower than those reported in the present work and Ref. [24], for FG-O, the natural frequencies demonstrated by Ref. [7] are greater than those reported in the present work and

Table 2
The dimensionless frequency parameters of a plate enriched with GNPs with no agglomeration.

(m,n)		Theory	UD	FG-V	FG-O	FG-X
(1,1)	Present	Quasi-3D HSDT	0.1218	0.1125	0.0968	0.1401
	Afshari and Adab [24]	Quasi-3D SSDT	0.1222	0.1127	0.0971	0.1402
	Song et al. [7]	FSDT	0.1216	0.1118	0.1020	0.1378
(2,1)	Present	Quasi-3D HSDT	0.2907	0.2694	0.2350	0.3254
	Afshari and Adab [24]	Quasi-3D SSDT	0.2916	0.2701	0.2357	0.3253
	Song et al. [7]	FSDT	0.2895	0.2673	0.2456	0.3249
(2,2)	Present	Quasi-3D HSDT	0.4461	0.4148	0.3660	0.4890
	Afshari and Adab [24]	Quasi-3D SSDT	0.4477	0.4160	0.3671	0.4885
	Song et al. [7]	FSDT	0.4436	0.4110	0.3796	0.4939
(3,1)	Present	Quasi-3D HSDT	0.5436	0.5065	0.4497	0.5889
	Afshari and Adab [24]	Quasi-3D SSDT	0.5456	0.5080	0.4513	0.5881
	Song et al. [7]	FSDT	0.5400	0.5013	0.4645	0.5984
(3,2)	Present	Quasi-3D HSDT	0.6822	0.6372	0.5708	0.7279
	Afshari and Adab [24]	Quasi-3D SSDT	0.6849	0.6393	0.5728	0.7266
	Song et al. [7]	FSDT	0.6767	0.6299	0.5860	0.7454
(3,3)	Present	Quasi-3D HSDT	0.8961	0.8400	0.7617	0.9369
	Afshari and Adab [24]	Quasi-3D SSDT	0.8999	0.8430	0.7645	0.9374
	Song et al. [7]	FSDT	0.8869	0.8287	0.7755	0.9690

Ref. [24], and for FG-X, the natural frequencies provided by Ref. [7] are either lower or higher than those reported in the present work and Ref. [24]. To explain these discrepancies, it should be noticed that both stiffness and inertia of the plate (Eq. (23) and (27)) are affected by the employed plate theory. Thus, depending on the dispersion pattern of the GNPs, the natural frequencies estimated via quasi-3D shear deformation theories may be either lower or higher than those estimated via the FSDT.

For a plate with the FG-O dispersion pattern of the GNPs and subjected to the following uniformly scattered triangular pulse:

$$q(x,y,t)=\begin{cases}0.5\left(1-\dfrac{t}{0.01}\right) & MPa \quad 0\le t\le 0.01\ \mathrm{s}\\ 0 & \qquad t>0.01\ \mathrm{s}\end{cases}, \tag{44}$$

the dimensionless dynamic deflection is depicted in Fig. 4 a for two selected values of the GNPs percentage, and Fig. 4 b shows the corresponding result presented by Song et al. [7]. A comparison between these figures reveals the high precision of the illustrated work and the small discrepancy can be elucidated by the difference between the hired plate theories which are discussed in the free vibration analysis in Table 2.

6.3. Parametric examination

The impacts of the GNPs percentage on the dimensionless frequency parameters and dimensionless dynamic response of the plate are shown in Fig. 5a and 5b. Compared to the polymeric matrix, GNPs have lower density and higher shear and elastic moduli. Thus, adding GNPs to the matrix brings about higher extensional, shear, and flexural rigidities and lower mass inertia. As a result of these improvements, the dimensionless frequency parameters increase in all vibrational modes, and the dimensionless dynamic deflection diminishes by increasing the GNPs mass fraction.

Fig. 5 shows that by subjoining more and more GNPs to the polymeric matrix, their enriching effects and the percentage of improvement in the dynamic characteristics of the plate gradually decrease. Thus, due to the high price of GNPs, it is not an optimum design to use large amounts of them.

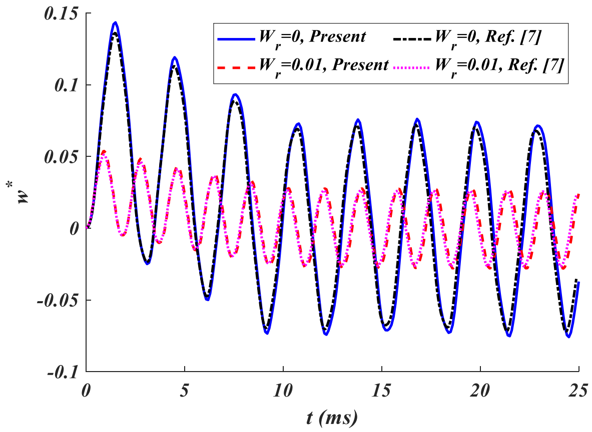

Fig. 4. The dimensionless dynamic deflection of a plate enriched with GNPs with no agglomeration.

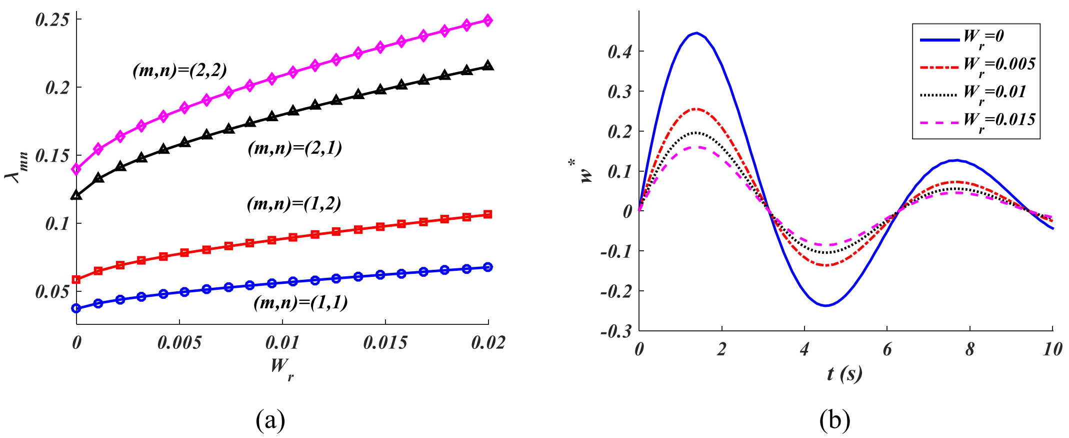

Fig. 5. The impacts of the GNPs percentage on (a) the dimensionless frequency parameters and (b) the dimensionless dynamic deflection.

Table 3
The influence of the dispersion pattern of the GNPs on the dimensionless frequency parameters.

	(m,n)			
	(1,1)	(1,2)	(2,1)	(2,2)
UD	0.0520	0.0821	0.1686	0.1962
FG-V	0.0502	0.0795	0.1633	0.1901
FG-O	0.0462	0.0732	0.1514	0.1765
FG-X	0.0562	0.0884	0.1798	0.2086

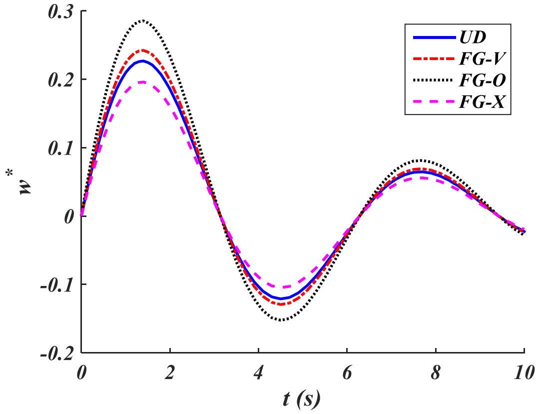

Fig. 6. The impact of the dispersion pattern of the GNPs on the dimensionless dynamic deflection.

Table 3 and Fig. 6 are demonstrated to discover the impacts of the dispersion pattern of the GNPs on the dimensionless frequency parameters and the dimensionless dynamic deflection. It can be declared that the lowest dimensionless frequency parameters and the highest dimensionless dynamic deflection belong to the FG-O dispersion pattern, and the highest dimensionless frequency parameters and the lowest dimensionless dynamic deflection belong to the FG-X dispersion pattern. Thus, to attain the highest enriching effects of the GNPs, it is more beneficial to dispense the majority of them near the surfaces ($z = \pm 0.5h$). Eq. (23) can be utilized to explain this improvement. As stated in this relation, growth in the elastic coefficients C_{11} and C_{22} at the surfaces of the plate leads to a higher flexural rigidity (coefficients A_4 and G_4). Thus, dispensing GNPs near the surfaces creates higher flexural rigidity which leads to higher natural frequencies and lower dynamic deflection.

Fig. 7a-8b are presented to examine the relevance of the dimensionless frequency parameters and the dimensionless dynamic deflection on the agglomeration parameters η and μ. Fig. 7a and 7 b reveals that growth in the agglomeration parameter η brings about lower dimensionless frequency parameters and a higher dimensionless dynamic deflection. As stated in Eq. (5) and Fig. 7a and 7b, it can be stated that when the amount of GNPs diminishes in the scattered regions and grows inside the clusters, their enriching effect is debilitated. The main reason for this deterioration is reductions in elastic and shear moduli of the GNP-reinforced polymer which reduce the extensional, shear, and flexural rigidities of the plate.

As observed in Fig. 8a and 8 b, growth in the agglomeration parameter μ brings about an enhancement in the dimensionless

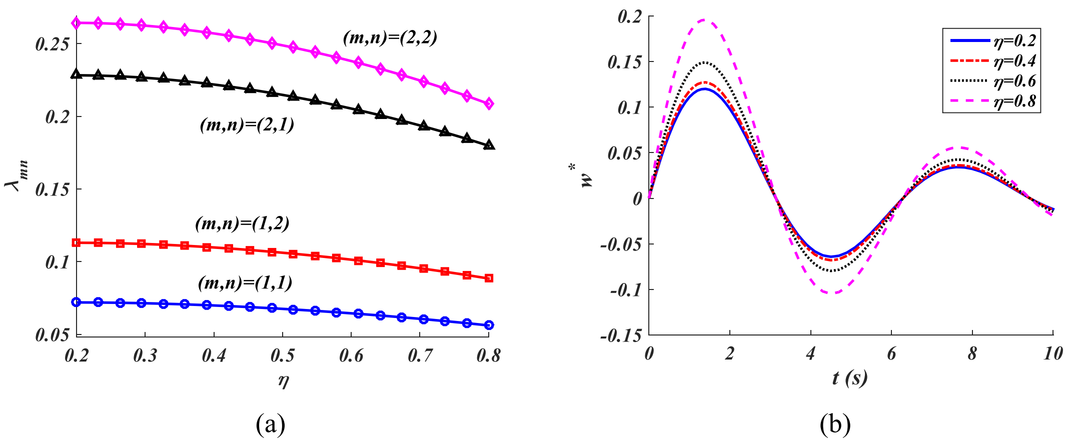

Fig. 7. The impact of agglomeration parameter η on (a) the dimensionless frequency parameters and (b) the dimensionless dynamic deflection.

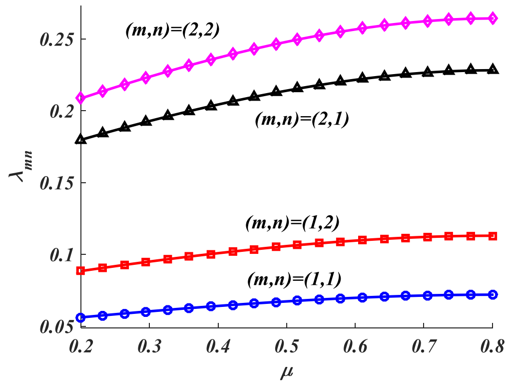

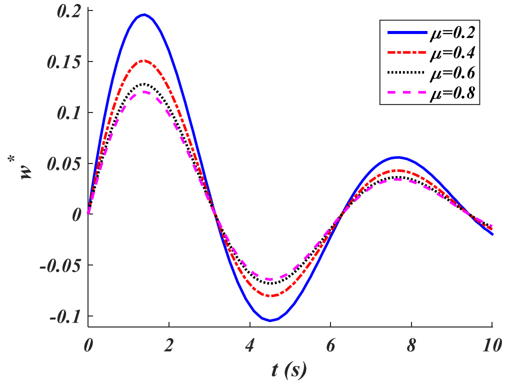

Fig. 8. The impact of agglomeration parameter μ on (a) the dimensionless frequency parameters and (b) the dimensionless dynamic deflection.

frequency parameters and a decrease in the dimensionless dynamic deflection. As stated in Eq. (5) and Fig. 8a and 8b, when the volume of each cluster increases, the compaction of aggregated GNPs decreases which declines the weakening impact of aggregation. The intensity of the agglomeration decreases by growing the agglomeration parameter μ. It raises the elastic and shear moduli of the GNP-reinforced polymer which brings about higher extensional, shear, and flexural rigidities of the plate.

7. Conclusions

The quasi-3D HSDT was employed and the vibration analyses of thick plates enriched with GNPs were examined. The agglomeration of the GNPs was incorporated and the mechanical characteristics were calculated via the Eshelby-Mori-Tanaka approach and the rule of mixture. An exact solution was provided via the Navier method. The most important findings of the presented work are listed in the statements below:

- Growth in the GNPs percentage brings about higher natural frequencies and a lower dynamic deflection.
- To attain the highest enriching effects of the GNPs, it is more beneficial to dispense the majority of them near the surfaces of the plate.
- For a specific GNPs percentage, growth in the amount of agglomerated GNPs brings about lower natural frequencies and higher dynamic deflection.
- For a specific mass fraction of the agglomerated GNPs, growth in the volume of the clusters brings about higher natural frequencies and lower dynamic deflection.

Author contribution statement

Ali alnujaie; Mohammad Yahya Alshahrani; Wessim Salahaddin Ibrahim: Conceived and designed the experiments; Wrote the paper.

Yaser Yasin; zahraa salam Obaid; Israa J. Alhani: Performed the experiments.

Mohammad Hasan Khaddour; Salema K. Hadrawi: Analyzed and interpreted the data.

Yassine Riyahi; M.H. Ghazwani: Contributed reagents, materials, analysis tools or data.

Data availability statement

Data included in article/supplementary material/referenced in article.

Additional information

No additional information is available for this paper.

Declaration of Competing interest

The authors declare that they have no known competing financial interests or personal relationships that could have appeared to influence the work reported in this paper.

Acknowledgments

The authors are grateful to Scientific Research Deanship at King Khalid University, Abha, Saudi Arabia for their financial support through the Large Research Group Project under grant number (RGP. 02-227-43). The authors extend their appreciation to the Deputyship for Research & Innovation, Ministry of Education in Saudi Arabia for funding this research work through the project number ISP23-64.

References

[1] M.H. Hajmohammad, M.B. Azizkhani, R. Kolahchi, Multiphase nanocomposite viscoelastic laminated conical shells subjected to magneto-hygrothermal loads: dynamic buckling analysis, Int. J. Mech. Sci. 137 (2018) 205–213.
[2] A. Farrokhian, M. Salmani-Tehrani, Surface and small scale effects on the dynamic buckling of carbon nanotubes with smart layers assuming structural damping, Steel and Composite Structures, Int. J. 37 (2) (2020) 229–251.
[3] M.A. Rafiee, J. Rafiee, Z. Wang, H. Song, Z.-Z. Yu, N. Koratkar, Enhanced mechanical properties of nanocomposites at low graphene content, ACS Nano 3 (12) (2009) 3884–3890.
[4] H. Adam, Carbon fibre in automotive applications, Mater. Des. 18 (4–6) (1997) 349–355.
[5] S. Bellucci, C. Balasubramanian, F. Micciulla, G. Rinaldi, CNT composites for aerospace applications, J. Exp. Nanosci. 2 (3) (2007) 193–206.
[6] F. Gauvin, M. Robert, Durability study of vinylester/silicate nanocomposites for civil engineering applications, Polym. Degrad. Stabil. 121 (2015) 359–368.
[7] M. Song, S. Kitipornchai, J. Yang, Free and forced vibrations of functionally graded polymer composite plates reinforced with graphene nanoplatelets, Compos. Struct. 159 (2017) 579–588.
[8] M. Song, J. Yang, S. Kitipornchai, Bending and buckling analyses of functionally graded polymer composite plates reinforced with graphene nanoplatelets, Compos. B Eng. 134 (2018) 106–113.
[9] M.R. Barati, A.M. Zenkour, Vibration Analysis of Functionally Graded Graphene Platelet Reinforced Cylindrical Shells with Different Porosity Distributions, Mechanics of Advanced Materials and Structures, 2018, pp. 1–9.
[10] S. Sahmani, M.M. Aghdam, T. Rabczuk, A unified nonlocal strain gradient plate model for nonlinear axial instability of functionally graded porous micro/nano-plates reinforced with graphene platelets, Mater. Res. Express 5 (4) (2018), 045048.
[11] Q. Li, D. Wu, X. Chen, L. Liu, Y. Yu, W. Gao, Nonlinear vibration and dynamic buckling analyses of sandwich functionally graded porous plate with graphene platelet reinforcement resting on Winkler–Pasternak elastic foundation, Int. J. Mech. Sci. 148 (2018) 596–610.
[12] Y. Wang, C. Feng, Z. Zhao, F. Lu, J. Yang, Torsional buckling of graphene platelets (GPLs) reinforced functionally graded cylindrical shell with cutout, Compos. Struct. 197 (2018) 72–79.
[13] R. Gholami, R. Ansari, Nonlinear harmonically excited vibration of third-order shear deformable functionally graded graphene platelet-reinforced composite rectangular plates, Eng. Struct. 156 (2018) 197–209.
[14] M. Safarpour, A. Rahimi, A. Alibeigloo, Static and Free Vibration Analysis of Graphene Platelets Reinforced Composite Truncated Conical Shell, Cylindrical Shell, and Annular Plate Using Theory of Elasticity and DQM, Mechanics Based Design of Structures and Machines, 2019, pp. 1–29.
[15] S. Qaderi, F. Ebrahimi, V. Mahesh, Free vibration analysis of graphene platelets–reinforced composites plates in thermal environment based on higher-order shear deformation plate theory, International Journal of Aeronautical and Space Sciences (2019) 1–11.
[16] A.R. Saidi, R. Bahaadini, K. Majidi-Mozafari, On vibration and stability analysis of porous plates reinforced by graphene platelets under aerodynamical loading, Compos. B Eng. 164 (2019) 778–799.
[17] Y.Q. Wang, Y.F. Liu, J. Zu, Size-dependent vibration of circular cylindrical polymeric microshells reinforced with graphene platelets, International Journal of Applied Mechanics 11 (4) (2019), 1950036.
[18] Y.Q. Wang, C. Ye, J.W. Zu, Nonlinear vibration of metal foam cylindrical shells reinforced with graphene platelets, Aero. Sci. Technol. 85 (2019) 359–370.
[19] H. Afshari, Free vibration analysis of GNP-reinforced truncated conical shells with different boundary conditions, Aust. J. Mech. Eng. 20 (5) (2022) 1363–1378.
[20] H. Afshari, Effect of graphene nanoplatelet reinforcements on the dynamics of rotating truncated conical shells, J. Braz. Soc. Mech. Sci. Eng. 42 (2020) 519.
[21] M. Al-Furjan, A. Farrokhian, S. Mahmoud, R. Kolahchi, Dynamic deflection and contact force histories of graphene platelets reinforced conical shell integrated with magnetostrictive layers subjected to low-velocity impact, Thin-Walled Struct. 163 (2021), 107706.
[22] M. Arefi, N. Adab, Coupled Stress Based Formulation for Static and Dynamic Analyses of a Higher-Order Shear and Normal Deformable FG-GPL Reinforced Microplates, Waves in Random and Complex Media, 2021, pp. 1–26.
[23] M.K. Nasution, R. Syah, D. Ramdan, H. Afshari, H. Amirabadi, M.M. Selim, A. Khan, M.L. Rahman, M.S. Sarjadi, C.-H. Su, Modeling and computational simulation for Supersonic flutter prediction of polymer/GNP/fiber laminated composite joined conical-conical shells, Arab. J. Chem. 15 (1) (2022), 103460.
[24] H. Afshari, N. Adab, Size-dependent buckling and vibration analyses of GNP reinforced microplates based on the quasi-3D sinusoidal shear deformation theory, Mech. Base. Des. Struct. Mach. 50 (1) (2022) 184–205.
[25] N. Adab, M. Arefi, Vibrational behavior of truncated conical porous GPL-reinforced sandwich micro/nano-shells, Eng. Comput. (2022) 1–25.
[26] N. Adab, M. Arefi, M. Amabili, A comprehensive vibration analysis of rotating truncated sandwich conical microshells including porous core and GPL-reinforced face-sheets, Compos. Struct. 279 (2022), 114761.
[27] J. Fang, B. Yin, L. Li, D. Zhang, Thermal buckling and vibration analysis of rotating porous FG GNPs-reinforced Reddy microplates, Aero. Sci. Technol. (2023), 108298.
[28] M. Sarafraz, H. Seidi, F. Kakavand, N.S. Viliani, Flutter characteristics of a rectangular sandwich plate with laminated three-phase polymer/GNP/fiber face sheets and an auxetic honeycomb core in yawed supersonic fluid flow, J. Braz. Soc. Mech. Sci. Eng. 45 (4) (2023) 197.
[29] M. Sarafraz, H. Seidi, F. Kakavand, N.S. Viliani, Free vibration and buckling analyses of a rectangular sandwich plate with an auxetic honeycomb core and laminated three-phase polymer/GNP/fiber face sheets, Thin-Walled Struct. 183 (2023), 110331.
[30] Y. Wang, W. Zhang, On the thermal buckling and postbuckling responses of temperature-dependent graphene platelets reinforced porous nanocomposite beams, Compos. Struct. 296 (2022), 115880.
[31] W. Zhang, C. Wang, Y. Wang, Thermo-mechanical analysis of porous functionally graded graphene reinforced cylindrical panels using an improved third order shear deformable model, Appl. Math. Model. 118 (2023) 453–473.
[32] H. Hedayati, B.S. Aragh, Influence of graded agglomerated CNTs on vibration of CNT-reinforced annular sectorial plates resting on Pasternak foundation, Appl. Math. Comput. 218 (17) (2012) 8715–8735.
[33] F. Tornabene, M. Bacciocchi, N. Fantuzzi, J. Reddy, Multiscale approach for three-phase CNT/polymer/fiber laminated nanocomposite structures, Polym. Compos. 40 (S1) (2019) E102–E126.
[34] A.R. Ghasemi, M. Mohandes, R. Dimitri, F. Tornabene, Agglomeration effects on the vibrations of CNTs/fiber/polymer/metal hybrid laminates cylindrical shell, Compos. B Eng. 167 (2019) 700–716.
[35] A.H. Yousefi, P. Memarzadeh, H. Afshari, S.J. Hosseini, Agglomeration effects on free vibration characteristics of three-phase CNT/polymer/fiber laminated truncated conical shells, Thin-Walled Struct. 157 (2020), 107077.
[36] A.H. Yousefi, P. Memarzadeh, H. Afshari, S.J. Hosseini, Optimization of CNT/polymer/fiber laminated truncated conical panels for maximum fundamental frequency and minimum cost, Mech. Base. Des. Struct. Mach. (2021) 1–23.
[37] A.H. Yousefi, P. Memarzadeh, H. Afshari, S.J. Hosseini, Dynamic Characteristics of Truncated Conical Panels Made of FRPs Reinforced with Agglomerated CNTs, Structures, Elsevier, 2021, pp. 4701–4717.

[38] H. Afshari, H. Amirabadi, Vibration characteristics of rotating truncated conical shells reinforced with agglomerated carbon nanotubes, J. Vib. Control 28 (15–16) (2022) 1894–1914.
[39] H. Afshari, Y. Ariaseresht, S.S. Rahimian Koloor, H. Amirabadi, M.O. Bidgoli, Supersonic Flutter Behavior of a Polymeric Truncated Conical Shell Reinforced with Agglomerated CNTs, Waves in Random and Complex Media, 2022, pp. 1–25.
[40] F. Kiani, Y. Ariaseresht, A. Niroumand, H. Afshari, Thermo-mechanical buckling analysis of thick beams reinforced with agglomerated CNTs with temperature-dependent thermo-mechanical properties under a nonuniform thermal loading, Mech. Base. Des. Struct. Mach. (2022) 1–21.
[41] A. Farrokhian, Buckling response of smart plates reinforced by nanoparticles utilizing analytical method, steel and composite structures, Int. J. 35 (1) (2020) 1–12.
[42] X.-Y. Ji, Y.-P. Cao, X.-Q. Feng, Micromechanics prediction of the effective elastic moduli of graphene sheet-reinforced polymer nanocomposites, Model. Simulat. Mater. Sci. Eng. 18 (4) (2010), 045005.
[43] E. García-Macías, L. Rodriguez-Tembleque, A. Sáez, Bending and free vibration analysis of functionally graded graphene vs. carbon nanotube reinforced composite plates, Compos. Struct. 186 (2018) 123–138.
[44] E. Sobhani, A.R. Masoodi, O. Civalek, A.R. Ahmadi-Pari, Agglomerated impact of CNT vs. GNP nanofillers on hybridization of polymer matrix for vibration of coupled hemispherical-conical-conical shells, Aero. Sci. Technol. 120 (2022), 107257.
[45] Y. Wang, H. Ma, K. Xie, T. Fu, J. Chen, Y. Liu, Nonlinear bending of a sandwich beam with metal foam and GPLRC face-sheets using Chebyshev–Ritz method: effects of agglomeration and internal pore, Thin-Walled Struct. 181 (2022), 110035.
[46] H. Golabchi, R. Kolahchi, M.R. Bidgoli, Vibration and instability analysis of pipes reinforced by SiO2 nanoparticles considering agglomeration effects, Comput. Concrete Int. J. 21 (4) (2018) 431–440.
[47] A. Farrokhian, The effect of voltage and nanoparticles on the vibration of sandwich nanocomposite smart plates, steel and composite structures, Int. J. 34 (5) (2020) 733–742.
[48] J.D. Eshelby, The determination of the elastic field of an ellipsoidal inclusion, and related problems, Proc. R. Soc. Lond. A Math. Phys. Sci. 241 (1226) (1957) 376–396.
[49] T. Mori, K. Tanaka, Average stress in matrix and average elastic energy of materials with misfitting inclusions, Acta Metall. 21 (5) (1973) 571–574.
[50] D.-L. Shi, X.-Q. Feng, Y.Y. Huang, K.-C. Hwang, H. Gao, The effect of nanotube waviness and agglomeration on the elastic property of carbon nanotube-reinforced composites, J. Eng. Mater. Technol. 126 (3) (2004) 250–257.
[51] H.-T. Thai, T.P. Vo, T.Q. Bui, T.-K. Nguyen, A quasi-3D hyperbolic shear deformation theory for functionally graded plates, Acta Mech. 225 (3) (2014) 951–964.
[52] N.M. Newmark, A method of computation for structural dynamics, J. Eng. Mech. Div. 85 (3) (1959) 67–94.
[53] J.H. Affdl, J. Kardos, The Halpin-Tsai equations: a review, Polym. Eng. Sci. 16 (5) (1976) 344–352.